IOPscience iopscience.iop.org

Home Search Collections Journals About Contact us My IOPscience

Role of triaxiality in ^{76}Ge and ^{76}Se nuclei studied with Gogny energy density functionals

This content has been downloaded from IOPscience. Please scroll down to see the full text.

2017 J. Phys. G: Nucl. Part. Phys. 44 034002

(http://iopscience.iop.org/0954-3899/44/3/034002)

View the table of contents for this issue, or go to the journal homepage for more

Download details:

IP Address: 130.83.108.230
This content was downloaded on 29/06/2017 at 14:38

Please note that terms and conditions apply.

You may also be interested in:

State-of-the-art of beyond mean field theories with nuclear density functionals
J Luis Egido

Collective motion in complex nuclei
Tomás R Rodríguez and J Luis Egido

Coexistence of nuclear shapes: self-consistent mean-field and beyond
Z P Li, T Nikši and D Vretenar

Status and future of nuclear matrix elements for neutrinoless double-beta decay: a review
Jonathan Engel and Javier Menéndez

Projection techniques to approach the nuclear many-body problem
Yang Sun

Role of triaxiality in the ground-state shape of neutron-rich Yb, Hf, W, Os and Pt isotopes
L M Robledo, R Rodríguez-Guzmán and P Sarriguren

Nuclear chiral and magnetic rotation in covariant density functional theory
Jie Meng and Pengwei Zhao

Microscopic theory of nuclear fission: a review
N Schunck and L M Robledo

Review of the properties of the 0\nu\beta - \beta - nuclear matrix elements
Jouni Suhonen and Osvaldo Civitarese

IOP Publishing Journal of Physics G: Nuclear and Particle Physics
J. Phys. G: Nucl. Part. Phys. **44** (2017) 034002 (14pp) https://doi.org/10.1088/1361-6471/aa57d3

Role of triaxiality in ^{76}Ge and ^{76}Se nuclei studied with Gogny energy density functionals

Tomás R Rodríguez[1]

Departamento de Física Teórica, Universidad Autónoma de Madrid, E-28049, Madrid, Spain

E-mail: tomas.rodriguez@uam.es

Received 20 August 2016, revised 6 January 2017
Accepted for publication 9 January 2017
Published 2 February 2017

Abstract

The structure of the nuclei ^{76}Ge and ^{76}Se is studied with symmetry conserving configuration mixing methods based on the Gogny D1S interaction. These two nuclei are of key importance in the search for neutrinoless double-beta decay. The energy density functionals used here include symmetry restorations (particle number and angular momentum) and shape mixing within the generator coordinate method. The comparison with the experimental data shows a good qualitative agreement when triaxial shapes are included, revealing the important role played by this degree of freedom in these two nuclei.

Keywords: energy density functionals, triaxiality, double beta decay

(Some figures may appear in colour only in the online journal)

1. Introduction

Detailed study of the structure of the ^{76}Ge and ^{76}Se isobars has been recently fostered by the fact that they are the initial and final nuclei in a potential neutrinoless double beta decay ($0\nu\beta\beta$). In this lepton number violating process, the initial nucleus decays to the final nucleus with two protons more and two neutrons less, and only two electrons are emitted. This mechanism is only possible if neutrinos are Majorana particles and its detection will help to disentangle the absolute neutrino mass and the neutrino mass hierarchy problem [1–3].

[1] This article belongs to the Special Issue: Emerging Leaders, which features invited work from the best early-career researchers working within the scope of J Phys G. This project is part of the *Journal of Physics* series' 50th anniversary celebrations in 2017. Tomàs Rodrìguez was selected by the Editorial Board of J Phys G as an Emerging Leader.

 © 2017 IOP Publishing Ltd Printed in the UK

Therefore, this is one of the most promising processes to detect physics beyond the Standard Model without using colliders. In the most plausible mechanism, i.e., the exchange of a light Majorana neutrino, the inverse of the half-life of the $0\nu\beta\beta$ decay is proportional to a kinematic phase space factor, the effective Majorana neutrino mass and the so-called nuclear matrix element (NME) that accounts for the probability of connecting the ground states of the initial and final nuclei [2].

The NMEs of the dozen of potential $0\nu\beta\beta$ decays have been calculated using different state-of-the-art nuclear many-body techniques such as the large scale shell model (LSSM) [4–8], the quasiparticle random phase approximation (QRPA) [9–12], the interacting boson model (IBM) [13, 14] and energy density functionals (EDFs) [15–18]. Currently, the discrepancies between the values of the NMEs given by those methods are roughly within a factor of three [19, 20]. This is a serious limiting factor for: (a) the design of the experiments aimed at detecting $0\nu\beta\beta$ decays, and, (b) studying the effective neutrino mass and mass hierarchy accurately if this decay is eventually detected.

Nevertheless, in the last few years the dependence of the NMEs on some of the most relevant nuclear degrees of freedom has been analyzed. These studies allow for a better constraint on these quantities and they also test the reliability of the different methods. Hence, the role of the deformation [15, 21–24], pairing and seniority [4, 10, 16, 25], isospin symmetry breaking [26–28], model space [8, 12, 29], closure versus non-closure approximation [30, 31], etc, has been established both in the potential candidates and in isotopic chains [27, 32, 33]. For example, it has been shown that the NMEs are enhanced (suppressed) when initial and final states have similar (different) deformations. Moreover, the NMEs are larger when spherical symmetry is assumed for the intrinsic initial and final states.

The search for $0\nu\beta\beta$ decays in the nucleus ^{76}Ge to the isobar ^{76}Se is currently the subject of two major experiments, namely, GERDA [34] and MAJORANA [35]. The predictions for the NME range from $\sim$2–3 given by LSSM to $\sim$5–6 predicted by QRPA and EDF approaches.

As a step towards providing a more reliable NME for this decay within EDF methods, it is the purpose of this work to study the structure of these two nuclei with symmetry conserving configuration methods (SCCMs) [36–38] based on the Gogny D1S interaction [39]. In particular, the role of the triaxial deformation is analyzed in detail since all the calculations of the NMEs performed with EDF approaches have assumed axial symmetry. In addition, the occupation numbers of spherical orbits [40] are calculated to show which are the most relevant. This kind of study could serve as a guide to defining the valence space in future LSSM/IBM/QRPA calculations with two-body interactions.

From an experimental point of view, strong indications of triaxiality in ^{76}Ge have been found in above-barrier Coulomb excitation and inelastic scattering experiments [41]. In particular, both the staggering parameter in the γ-band and the ratios between different reduced electromagnetic transition probabilities are consistent with a rigid-γ deformed nucleus. These results are well described qualitatively by the phenomenological model of Davydov and Filippov [42] as well as quantitatively with more microscopic methods such as the shell model [41], the triaxial projected shell model [43], the proton–neutron IBM [44] and the relativistic EDF based on a collective Hamiltonian [45]. The latter calculation shows also signatures of γ-softness instead of a rigid-γ character.

Fingerprints of triaxiality, such as the presence of a low-lying γ-band, have been also observed in the ^{76}Se nucleus [46–48]. The low-lying spectrum is quite well reproduced by the triaxial projected shell model [43], IBM [49] and the collective Hamiltonian based on a Skyrme interaction [50]. Self-consistent mean-field calculations in the triaxial plane with Skyrme [50] and Gogny [51] interactions predict a γ-soft nucleus with the minimum of the

potential energy surface (PES) located at an axial oblate configuration. This oblate character is also predicted by axially symmetric SCCM calculations with Gogny [52] and relativistic Lagrangians [18]. However, the experimental spectroscopic quadrupole moment of the first 2^+ excited state has a negative sign, contrary to the self-consistent mean-field and axial SCCM results. This fact could indicate the relevance of both correlations beyond the mean-field approximation and triaxiality.

Apart from excitation energies and electromagnetic properties, experiments with nucleon transfer/removal reactions have been performed in the last few years to pin down the most relevant spherical single particle orbits in ^{76}Ge and ^{76}Se [53, 54]. Occupation numbers of spherical orbits are not observables and the comparison between the results provided by different nuclear many-body methods must be taken with caution [55]. However, this information about the structure of the nuclei can be used to provide additional confidence on the theoretical method [56] and/or constrain the parameters used in the calculation of $0\nu\beta\beta$ NMEs [57, 58].

This paper is organized as follows. First, a brief review of the SCCM methods used in this work is given in section 2. Then, the main results of the calculations are given in section 3 where the PESs, excitation energies, electromagnetic properties, collective wave functions (c.w.f.s) and occupation numbers are discussed. Finally, section 4 is devoted to a summary of the main findings of the present study and gives an outlook for future work.

2. Outline of the SCCM methods

In this section the SCCM method used here is summarized. A much more detailed description of the method can be found in [36–38]. In this approach, based on the variational principle, the nuclear many-body states are defined as linear combinations of product-like wave functions which are projected onto a good number of protons (Z) and neutrons (N), and the total angular momentum and its third component (J, M):

$$|JM; NZ; \sigma\rangle = \sum_{\beta_2,\gamma,K} f^{J\sigma}_{\beta_2,\gamma,K} |JMK; NZ; \beta_2, \gamma\rangle. \tag{1}$$

Here, $\sigma = 1, 2, \ldots$ are the labels for the different states having a given angular momentum. The above definition corresponds to the generator coordinate method (GCM) ansatz [59]. The projected wave functions are defined as [59]:

$$|JMK; NZ; \beta_2, \gamma\rangle = P^J_{MK} P^N P^Z |\beta_2, \gamma\rangle, \tag{2}$$

where P^J_{MK} is the angular momentum projector and $K = -J, -J+1, \ldots, J$ is the component of the angular momentum in the body-fixed z-axis. The intrinsic product-like states, $|\beta_2, \gamma\rangle \equiv |\rangle$, are calculated with the variation after particle number projection (PN-VAP) method [60], i.e., minimizing the particle number projected energy with constraints:

$$E'(\beta_2, \gamma) = E(\beta_2, \gamma) - \lambda_{q_{20}} \langle \hat{Q}_{20} \rangle - \lambda_{q_{22}} \langle \hat{Q}_{22} \rangle, \tag{3}$$

$$E(\beta_2, \gamma) = \frac{\langle \hat{H} P^N P^Z \rangle}{\langle P^N P^Z \rangle}. \tag{4}$$

Here, $P^{N(Z)}$ is the neutron (proton) projection operator [59]. The constraints in equation (3) are the degrees of freedom explored explicitly by the nuclear states in equation (1), and $\lambda_{q_{20}}$, $\lambda_{q_{22}}$ are the Lagrange multipliers that ensure the conditions:

$$\langle \hat{Q}_{20} \rangle = q_{20}; \langle \hat{Q}_{22} \rangle = q_{22}, \tag{5}$$

where $\hat{Q}_{2\mu}$ with $\mu = -2, -1, .., 2$ is the μ component of the quadrupole operator. The deformation parameters mentioned above are defined as:

$$q_{20} = \frac{\beta_2 \cos\gamma}{C}; \; q_{22} = \frac{\beta_2 \sin\gamma}{\sqrt{2}\,C}; \; C = \sqrt{\frac{5}{4\pi}} \frac{4\pi}{3r_0^2 A^{5/3}} \tag{6}$$

being A the mass number and $r_0 = 1.2$ fm.

Finally, the coefficients $f^{J\sigma}_{\beta_2,\gamma,K}$ in equation (1) are found by minimizing the energy obtained from these GCM states, leading to the Hill–Wheeler–Griffin (HWG) equations [59]:

$$\sum_{\{\alpha'\}} (\mathcal{H}^{J;NZ}_{\{\alpha\};\{\alpha'\}} - E^{J\sigma} \mathcal{N}^{J;NZ}_{\{\alpha\};\{\alpha'\}}) f^{J\sigma}_{\{\alpha'\}} = 0, \tag{7}$$

where $\{\alpha\} \equiv \{\beta_2, \gamma, K\}$ and $\mathcal{H}$ and $\mathcal{N}$ are the energy and norm overlaps, respectively:

$$\mathcal{N}^{J;NZ}_{\{\alpha\};\{\alpha'\}} = \langle JMK; NZ; \beta_2, \gamma | JMK'; NZ; \beta_2', \gamma' \rangle, \tag{8}$$

$$\mathcal{H}^{J;NZ}_{\{\alpha\};\{\alpha'\}} = \langle JMK; NZ; \beta_2, \gamma | \hat{H} | JMK'; NZ; \beta_2', \gamma' \rangle. \tag{9}$$

Once equation (7) is solved, not only is the energy spectrum ($E^{J\sigma}$) obtained, but also the many-body wave functions that can be used to compute expectation values, transition probabilities and NMEs (see [15, 36–38, 61, 62] for more details).

Self-consistent symmetries can be imposed in the definition of the product-like (intrinsic) wave functions in order to reduce both the complexity of the method and, more importantly, the computational cost [63]. In this work, parity is conserved and therefore only positive parity states can be described. Additionally, time-reversal symmetry is conserved, largely simplifying the calculations at the cost of exploring the ground state variationally better than the excited states [64]. The main effect of this restriction is a stretching of the predicted spectra. One can further simplify the SCCM method by including only product-like states with axial symmetry, i.e., $\gamma = 0°$ (prolate) and $\gamma = 60°$ (oblate, or equivalently negative values of β_2 or $\gamma = 180°$). In this case, only nuclear states with $K = 0$ and J-even can be computed, which is a severe limitation to describe, for example, γ-soft or triaxial rotor nuclei, or γ-bands. However, due to its simplicity, the axial approach has been assumed in the calculations of $0\nu\beta\beta$ NMEs of the $A = 76$ decay performed so far with SCCM methods [15, 16, 18].

In this work, the number of intrinsic states included in the definition of the GCM states (equation (1)) is 15 and 60 for the axial and triaxial approximations, respectively. A good convergence of the energies after solving the HWG equations is obtained with this choice. These product-like states are defined in a spherical harmonic oscillator basis with nine major shells. In addition, the number of gauge (particle number projection) and Euler (angular momentum projection) angles are 9 and 2048 respectively, suitable for correctly reproducing the expectation values of the number of particles and the total angular momentum operator $\hat{J}^2$. Finally, the Gogny D1S parametrization has been used in all the cases. More technical details about the calculations are explained in [37].

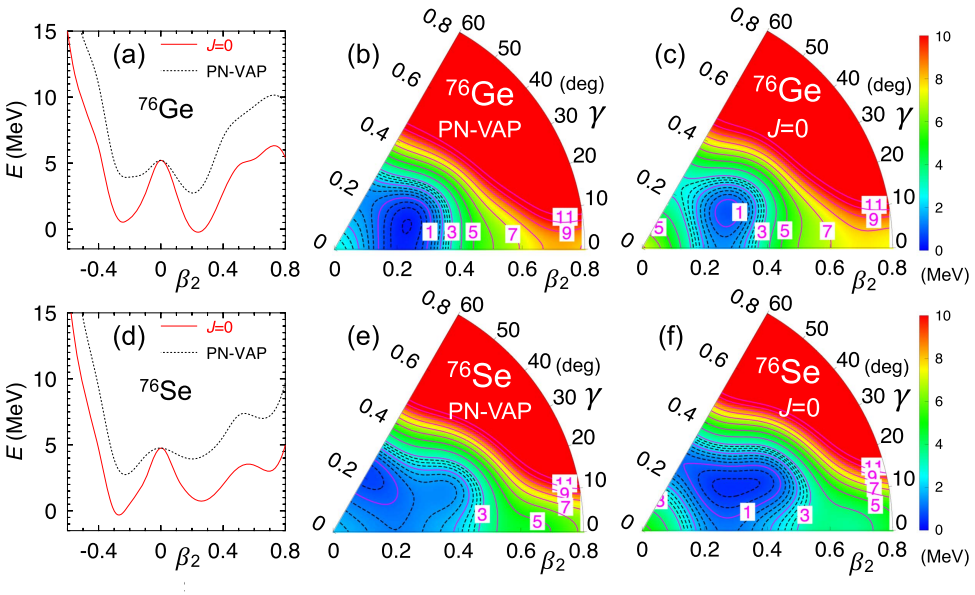

Figure 1. Particle number (PN-VAP) and particle number and angular momentum (PNAMP, $J = 0$) projected potential energy surfaces for (a)–(c) ^{76}Ge and (d)–(f) ^{76}Se calculated with the Gogny D1S interaction. In the left panel, axial symmetry is assumed while in the central and right panels triaxial calculations are shown. Energies are normalized to the minimum of each surface (triaxial case) or to the minimum of the particle number and angular momentum projected energy (axial case).

3. Results

3.1. Potential energy surfaces

The collective behavior of the ground state of a nucleus can be normally inferred from the analysis of the PESs, i.e., the dependence of the energy on some collective variables like deformations and/or quantum fluctuations. These PESs can be evaluated with mean-field wave functions or with more sophisticated many-body states that include beyond-mean-field effects. In the present case, variation after particle number projected (PN-VAP) PES and particle number and angular momentum projected (PNAMP, $J = 0$) PES are plotted in figure 1 for the two isotopes studied here, namely, ^{76}Ge (figures 1(a)–(c)) and ^{76}Se (figures 1(d)–(f)).

In the axial case, the nucleus ^{76}Ge (figure 1(a)) shows a PN-VAP PES with two minima at $\beta_2 \approx \pm 0.2$, being the prolate one deeper, and a maximum at the spherical point. Once the angular momentum of the states is restored ($J = 0$), there is an energy gain for all the points except for the spherical state—which is a $J = 0$ eigenstate already at the PN-VAP level. The PNAMP PES presents a similar structure as before but with a slight displacement in the position of the minima towards a larger deformation. Therefore, in the axial approximation the nucleus ^{76}Ge is prolate deformed.

The results change if the γ degree of freedom is also explored. In figures 1(b)–(c) the PN-VAP and PNAMP energy surfaces in the (β_2, γ) plane are plotted. The PN-VAP PES shows a single minimum at $\approx$(0.25°, 15°) and a rather flat surface along the γ direction in the range of $\beta_2 \in [0.1, 0.3]$. The two minima observed in the axial PN-VAP PES are indeed saddle points

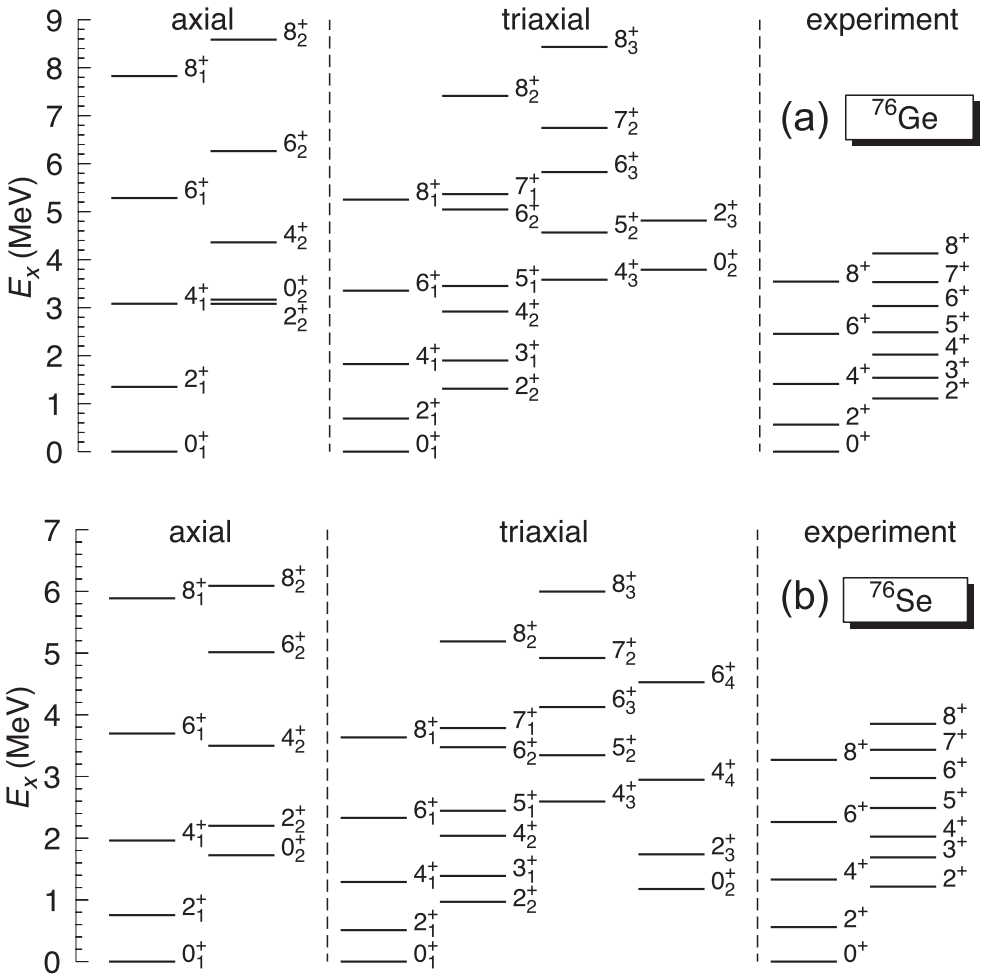

Figure 2. Theoretical and experimental spectra for (a) ^{76}Ge and (b) ^{76}Se nuclei. On the left, the axial approach is used and in the central panel triaxial calculations are shown. Experimental data are taken from [41, 48].

in the triaxial plane. The same happens with the PNAMP PES, where only one minimum is found at ≈(0.30°, 20°) and the two axial minima are saddle points. It is important to point out that this surface resembles the potential of a γ-rigid model.

Concerning the nucleus ^{76}Se, the changes are more significant when both triaxiality and angular momentum restoration are taken into account. In the axial PN-VAP and PNAMP approaches, and also in the triaxial PN-VAP PES, the absolute minima are obtained at an axial oblate configuration with $\beta_2 \approx -0.2$ ($\gamma = 60°$). However, the PNAMP PES shows a rather γ-soft behavior in the range of $\beta_2 \in [0.2, 0.4]$ and, for $\gamma \approx 25°$, in the interval $\beta_2 \in [0.2, 0.5]$. The absolute minimum is now displaced towards a more prolate value (0.3°, 25°), which is in fact more consistent with the negative sign of the experimental spectroscopic quadrupole moment $Q_{\rm sp}(2_1^+)$ [46].

The present analysis shows the relevance of the triaxial degree of freedom in these two isobars at this level of approximation. Nevertheless, the final nuclear states are obtained

Table 1. Experimental and theoretical (triaxial) ratios between the excitation energies $R_{4/2} = E(4_1^+)/E(2_1^+)$ and $R_{2/2} = E(2_2^+)/E(2_1^+)$, as well as the staggering parameters of the γ-band and the signs predicted by two geometrical models [42, 65, 66].

	$R_{4/2}$	$R_{2/2}$	$S(4)$	$S(5)$	$S(6)$	$S(7)$	$S(8)$
^{76}Ge (exp)	2.50	1.97	+0.09	−0.03	+0.15	−0.09	+0.17
^{76}Ge (triax)	2.65	1.90	+0.63	−0.71	+1.54	−1.85	+2.50
^{76}Se (exp)	2.38	2.17	−0.25	+0.23	+0.04	−0.05	−0.06
^{76}Se (triax)	2.53	1.90	+0.45	−0.48	+1.23	−1.41	+2.14
γ-soft	2.50	2.50	−	+	−	+	−
γ-rigid (30°)	2.60	2.00	+	−	+	−	+

within the SCCM method after performing the configuration mixing. This leap is necessary to compute energies and electromagnetic properties that can be directly compared with the experimental data. Additionally, theoretical objects like the c.w.f.s and the occupation numbers of spherical orbits can be studied to shed light on the structure of the different nuclear states. These topics will be discussed in the subsequent sections.

3.2. Energy levels

Ground state and excitation energies, $E^{J\sigma}$, are computed in the SCCM framework by solving the corresponding HWG equations (equation (7)). The results for the axial and triaxial calculations, as well as the experimental data, are shown in figure 2. In the axial case, the ground state bands are much more stretched than the experimental bands. This is understood in terms of the lack of both triaxiality and time-reversal symmetry breaking intrinsic states that produces a worse variational description of the excited states [37, 64]. In addition, the first excited bands of ^{76}Ge and ^{76}Se found experimentally are built on top of the 2_2^+ states with a $\Delta J = 1$ sequence. These γ-bands cannot be reproduced with axial calculations because only J-even states are allowed due to symmetry restrictions.

The comparison with the experimental data is much better when the triaxial degree of freedom is taken into account. The triaxial calculations predict in the two nuclei the presence of, apart from the ground state and γ-bands, two side bands: one with $\Delta J = 1$ built on top of the 4_3^+, and another one with $\Delta J = 2$ and a 0_2^+ band-head. As will be analyzed in section 3.4, the first band corresponds to a mostly $K = 4$ rotational band associated to the ground (mostly $K = 0$) and γ (mostly $K = 2$) bands. The character of the 0_2^+ band is different in ^{76}Ge and ^{76}Se. The latter is found at a smaller excitation energy and corresponds to an axial oblate rotational band while the former has an axial prolate character (see section 3.4 for more details).

Some fingerprints of the triaxial character of the nucleus are the ratios $R_{4/2} = E(4_1^+)/E(2_1^+)$ and $R_{2/2} = E(2_2^+)/E(2_1^+)$. The calculated and experimental values shown in table 1 are in fairly good agreement in both nuclei when the triaxial shapes are included. In addition, the way the states are distributed in the γ-band can distinguish between a γ-rigid or a γ-soft character of the nucleus [66]. This fact can be quantified by the staggering parameter:

$$S(J) = \frac{[E(J) - E(J-1)] - [E(J-1) - E(J-2)]}{E(2_1^+)}. \tag{10}$$

In table 1 the experimental and calculated values for $S(J)$, as well as the sign of this quantity predicted by a γ-rigid and a γ-soft model, are shown. In the case of ^{76}Ge, the experimental values and the theoretical ratios and staggering parameters are consistent with a γ-rigid

Table 2. Experimental and theoretical spectroscopic quadrupole moment (second column), magnetic dipole moment (third column) and $B(E2)$ reduced transition probabilities (fourth–seventh column) in units of e fm^2, nucleon magneton μ_N and W.u., respectively, for ^{76}Ge and ^{76}Se. Experimental values are taken from [67].

	$Q_{sp}(2_1^+)$	μ	$2_1^+ \rightarrow 0_1^+$	$2_2^+ \rightarrow 2_1^+$	$2_2^+ \rightarrow 0_1^+$	$4_1^+ \rightarrow 2_1^+$
^{76}Ge (axial)	−17.8	0.800	27.5	32.7	0.07	41.6
^{76}Ge (triax)	−20.4	0.763	38.5	48.9	0.25	56.3
^{76}Ge (exp)	−19 (6)	0.838 (46)	29 (1)	42 (9)	0.90 (22)	38 (9)
^{76}Se (axial)	+45.5	0.89	31.8	11.0	1.70	43.3
^{76}Se (triax)	−31.2	0.90	72.3	102.0	0.09	117.4
^{76}Se (exp)	−34 (7)	0.80 (22)	44 (1)	43 (3)	1.21 (10)	71 (2)

character while for ^{76}Se a more γ-soft character is obtained experimentally. In the latter nucleus, the triaxial calculations predict a more transitional character, with some of the ratios closer to γ-softness and some other quantities closer to a γ-rigid model. In section 3.4 the c.w. f.s will be analyzed to give a better understanding of the structure of these states.

Finally, it is important to give an estimation of the energy gain in the ground state by including the triaxial deformation in the SCCM method, i.e., $\Delta E_{\text{gain}} = E(0_1^+)_{\text{triax}} - E(0_1^+)_{\text{ax}}$. These values are $\Delta E_{\text{gain}} = 1.91$ MeV and 1.24 MeV for ^{76}Ge and ^{76}Se, respectively, showing again the relevance of this degree of freedom in these two isobars.

3.3. Electromagnetic transition probabilities and moments

The present SCCM methods allow for the calculation of the $B(E2)$ reduced transition probabilities as well as the electric spectroscopic quadrupole moments, Q_{sp}, and the magnetic dipole moment, μ. In table 2 the theoretical (axial and triaxial) and experimental values for the most relevant transitions are shown. For the nucleus ^{76}Ge, the spectroscopic quadrupole moment $Q_{\text{sp}}(2_1^+)$ is negative both experimentally and theoretically, indicating a prolate character, or, as it will be discussed in section 3.4, a value of $\gamma < 30°$. The reduced transition probabilities are large between the members of the ground state band ($2_1^+ \rightarrow 0_1^+$, $4_1^+ \rightarrow 2_1^+$) and also between the 2_2^+ and the 2_1^+ states. However, the transition between the band-head of the γ-band and the ground state is very small, which is again a hint of the triaxial character of this nucleus. The comparison between the theoretical results and the experiments reveals that the axial calculations reproduce the data reasonably well for the ground-state band while they underestimate the inter-band transitions. On the other hand, the triaxial calculations better reproduce those transitions although they predict systematically larger values for the in-band $B(E2)$'s.

Such an excess is more significant in the transition probabilities calculated for the nucleus ^{76}Se in the triaxial approach, probably due to an overestimation of the deformation given by the Gogny D1S in combination with the present SCCM method. Nevertheless, the same behavior of the $B(E2)$ as the one described above for the ^{76}Ge is also observed here, i.e., large transition probabilities within the ground state band and between the band-head of the γ-band and the 2_1^+ state, and a small transition $2_2^+ \rightarrow 0_1^+$.

However, the most interesting result is the change of sign in the spectroscopic quadrupole moment of the 2_1^+ state from an oblate character predicted by the axial calculation (Q_{sp} positive) to a more prolate character obtained when the triaxial shapes are included (Q_{sp} negative). The latter is indeed in agreement with the actual experimental value. As anticipated in section 3.1, this is an indication of both the important role of beyond-mean-field

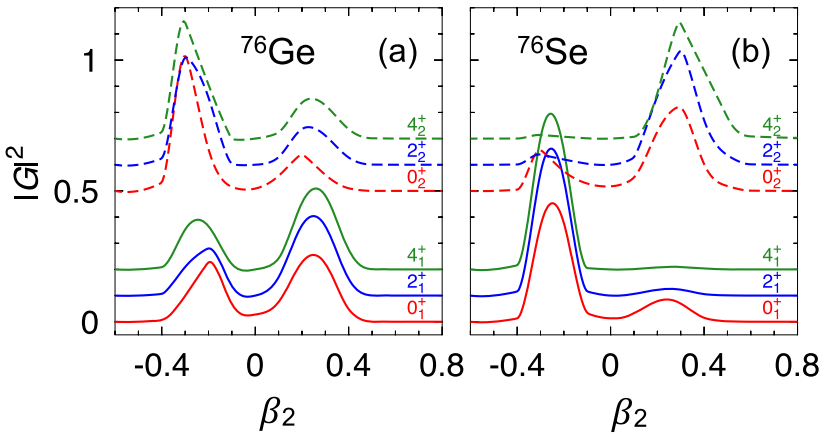

Figure 3. Collective wave functions for the states belonging to the ground state and first excited bands for (a) ^{76}Ge and (b) ^{76}Se nuclei obtained with axial SCCM calculations. The sum is normalized to 1 and the states different from 0_1^+ have been shifted for a better visualization.

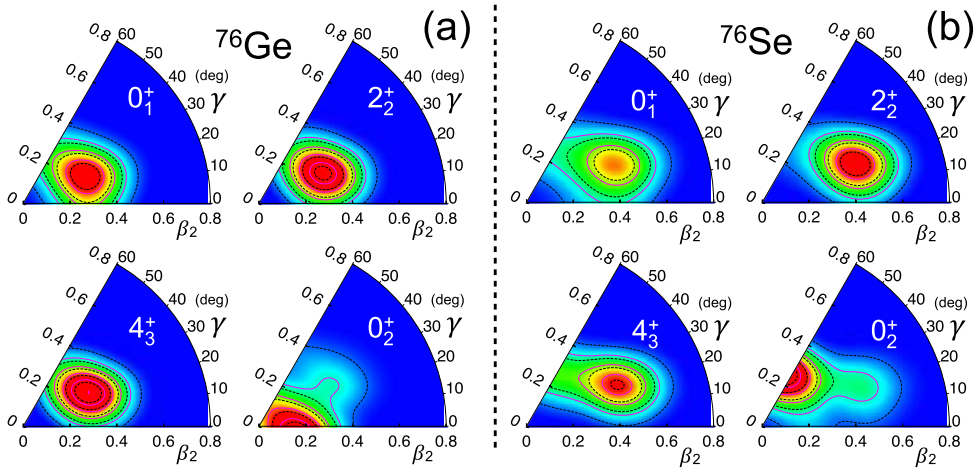

Figure 4. Collective wave functions for the band-head states of the ground state band, γ-band, second and third excited bands for (a) ^{76}Ge and (b) ^{76}Se nuclei obtained with triaxial SCCM calculations.

correlations associated to the angular momentum restoration, and the triaxiality in this nucleus. In the next section, this change of sign will be understood better with the analysis of the axial and triaxial wave functions.

3.4. Collective wave functions

In this section the so-called c.w.f.s obtained with axial and triaxial calculations are analyzed. These c.w.f.'s are orthonormal functions defined as [59]:

$$G^{J\sigma}(\beta_2,\,\gamma) = \sum_{K,\beta_2',\gamma,'K'} (\mathcal{N}^{J}_{\beta_2,\gamma K;\beta_2',\gamma',K'})^{1/2} f^{J\sigma}_{\beta_2',\gamma',K'}, \tag{11}$$

where $\mathcal{N}^{J}_{\beta_2,\gamma K;\beta_2',\gamma',K'}$ and $f^{J\sigma}_{\beta_2,\gamma,K}$ are defined in equations (8) and (1)m respectively. These functions represent the contribution of the intrinsic deformations in each nuclear state and they are very useful objects to study the collective character of the nucleus. As usual, the above expression is simplified in the axial approximation ($K = 0$ and $\gamma = 0°$ and $180°$).

Starting with the axial results, in figure 3 the c.w.f.'s for the lowest states of the ground state (0_1^+–4_1^+) and first excited (0_2^+–4_2^+) bands are shown. In fact, the states belonging to the same band, i.e., strongly connected by $B(E2)$ transitions, have a similar c.w.f.s. structures. In both nuclei the c.w.f.'s are basically located at the wells of the PES shown in figures 1(a) and (d). Hence, the ground state band of ^{76}Ge (figure 3(a)) is an admixture of prolate and oblate configurations. Two peaks at $\beta_2 \approx \pm 0.25$ are obtained, with the prolate one a bit higher. The opposite situation is found in the first excited band where the oblate peak is much higher than the prolate one. Concerning the nucleus ^{76}Se (figure 3(b)), the shape mixing is considerable smaller -and negligible for angular momenta different from zero. In this case, the ground state band obtained with axial calculations has an oblate character with a peak at $\beta_2 \approx -0.25$ and the first excited band is mainly prolate deformed ($\beta_2 \approx +0.40$). Therefore, the calculated spectroscopic moment with the positive sign shown in table 2 is consistent with this picture.

As in the analysis of the PESs (section 3.1), the situation changes when the triaxial degree of freedom is included in the SCCM calculations. In figure 4 the c.w.f.'s for the band head states given in the middle panel of figure 2 are plotted. For both nuclei, the ground state, 0_1^+, the head of the γ-band, 2_2^+, and the head of the band, 4_3^+, show their maxima at triaxial shapes centered in $\gamma \approx 25°$. They are in fact the $K = 0$, 2 and 4 rotational bands built on top of practically the same deformation. These states are more deformed in the nucleus ^{76}Se ($\beta_2 \approx 0.4$) than in the nucleus ^{76}Ge ($\beta_2 \approx 0.3$). Furthermore, the ground state c.w.f. in ^{76}Se is more γ-soft than the one of ^{76}Ge, which shows a more γ-rigid character. These results are consistent with the energies and ratios discussed in section 3.2.

It is important to point out that the axial c.w.f.'s for the ground state bands shown in figure 3 are compatible with the axial path in the ground state c.w.f.'s in figure 4. That means that the maxima in the former c.w.f.'s at oblate and prolate deformations are indeed saddle points in the triaxial plane. However, the situation is more critical in the nucleus ^{76}Se since the inclusion of triaxial shapes changes the results of relevant observables such as the spectroscopic quadrupole moment of the 2_1^+. The c.w.f. of this state in the triaxial plane (not shown) is similar to the one of the ground state and has its maximum at a value of $\gamma < 30°$. Therefore, the calculated spectroscopic quadrupole moment is now negative, consistently with the experimental value.

Finally, the 0_2^+ states predicted by the triaxial calculations are also rather different from the axial results. An axial prolate ($\beta_2 \approx 0.15$) state and an axial oblate $\beta_2 \approx 0.25$ state are obtained for ^{76}Ge and ^{76}Se respectively, in clear contrast to the axial result shown in figure 3. Furthermore, rotational bands are built on top of these band-heads. The excitation energies of the 0_2^+,4_1^+ and 2_2^+ states in ^{76}Se are rather close (see figure 2(b)) and this fact could resemble a two-quadrupole phonon structure as obtained in IBM calculations [68]. However, the form of the 0_2^+ c.w.f.—and those belonging to the same band—does not support this interpretation in the present calculations. In addition, a structure associated to β-vibrations is obtained in ^{76}Ge and ^{76}Se at larger excitation energies. They are the 0_3^+ state in both nuclei (not shown). Therefore, these 0_2^+ states cannot be interpreted in terms of such a collective mode either.

3.5. Occupation numbers

The SCCM methods used throughout the paper provide a description of the nuclear states in terms of collective variables, like deformations, in a rather natural way. However, it is also useful to give more information of the structure in terms of a 'shell-model-like' language. To do so, the occupation numbers of spherical orbits have been calculated for the ground states of ^{76}Ge and ^{76}Se. Since in the SCCM methods all particles are active within a large harmonic oscillator single-particle basis, the first step consists in defining the spherical single-particle orbits that will be occupied by the nucleons. In the present case, these orbits are defined for each nucleus in a self-consistent manner from its spherically symmetric Hartree–Fock–Bogoliubov (HFB) solution. More specifically, the operator associated to the number of particles occupying a given spherical orbit, α, defined by the principal, orbital angular momentum and total angular momentum quantum numbers $(n_\alpha l_\alpha j_\alpha)$ is:

$$\hat{n}_\alpha = \sum_{m_{j_\alpha}} a^\dagger_{n_\alpha l_\alpha j_\alpha m_{j_\alpha}} a_{n_\alpha l_\alpha j_\alpha m_{j_\alpha}}. \tag{12}$$

These creation and annihilation single-particle operators $(a^\dagger_\alpha, a_\alpha)$ are obtained from the diagonalization of the one-body density-matrix that corresponds to the solution of an HFB calculation performed imposing spherical symmetry for the nucleus of interest [59]. Then, the above operator is used to evaluate the occupation numbers of the spherical orbits in the GCM nuclear states defined in equation (1) (see [40] for further details).

It is important to point out that the occupation numbers are not actual observables [55] but still they are useful quantities to test calculations and provide guidance for building physically sound valence spaces in LSSM, QRPA and/or IBM methods. These numbers can also give an insight of the relevance of the spin–orbit partners that are missing in most of the LSSM calculations for $0\nu\beta\beta$ NMEs. In particular, the valence space used in LSSM calculations in the $A = 76$ decay is made of the $0f_{5/2}$, $1p_{3/2}$, $1p_{1/2}$ and $0g_{9/2}$ orbits [56].

In table 3 the number of neutrons and protons occupying the *pf* and *gds* orbits are given for ^{76}Ge ($N = 44$, $Z = 32$) and ^{76}Se ($N = 42$, $Z = 34$). Both axial and triaxial calculations are shown. These occupation numbers reveal that both protons and neutrons do not show clear signatures of subshell closures. Hence, the $0f_{7/2}$ orbits are not fully occupied, specially in the proton case for the triaxial calculations. The filling of the neutron $0g_{9/2}$ orbit is also coming with a non-negligible occupancy of its quadrupole partner $1d_{5/2}$, and, to a lesser extent, of its spin–orbit partner $0g_{7/2}$. As mentioned above, these three orbits are out of the valence space in LSSM calculations. Although the renormalization of the nuclear interaction to produce shell model two-body matrix elements defined in a given reduced valence space could accommodate these missing orbits, it would be interesting to check in future LSSM calculations their influence both in the spectra and in the $0\nu\beta\beta$ NMEs.

The main difference between the axial and triaxial results is observed in the systematically larger occupancies of the *gds* orbits found in the latter case. Moreover, in table 3 the values inferred from nucleon transfer/removal experiments [53, 54] are also shown. Triaxial results are closer to the experimental values although the neutron $0f_{5/2}$ orbit is found to be more occupied and the neutron $0g_{9/2}$ orbit less occupied than the values extracted from the experiments. In addition, the proton $1p$ ($0f_{5/2}$) orbit is more (less) populated theoretically in ^{76}Se than in the experiments. On the other hand, such experiments are not sufficiently sensitive to explore occupancies in orbits above the $0g_{9/2}$ and vacancies in the $0f_{7/2}$ orbits that play a role in the calculations. Nevertheless, as mentioned above, the comparison between these non-observable quantities should be taken with caution since they contain several

Table 3. Occupation numbers of spherical orbits for the ground state of ^{76}Ge and ^{76}Se computed with axial and triaxial approximations. Experimental values are extracted from [53, 54].

Orbit	^{76}Ge ax	^{76}Ge triax	^{76}Ge exp	^{76}Se ax	^{76}Se triax	^{76}Se exp
$\nu 0f_{7/2}$	7.81	7.72	—	7.72	7.47	—
$\nu 1p$	5.38	4.88	4.87 ± 0.20	4.74	4.30	4.41 ± 0.20
$\nu 0f_{5/2}$	5.16	4.95	4.56 ± 0.40	4.96	4.24	3.83 ± 0.40
$\nu 0g_{9/2}$	4.65	4.84	6.48 ± 0.30	3.92	4.10	5.80 ± 0.30
$\nu 1d_{5/2}$	0.54	0.83	—	0.26	0.86	—
$\nu 0g_{7/2}$	0.16	0.24	—	0.19	0.31	—
$\nu 1d_{3/2}$	0.04	0.07	—	0.04	0.10	—
$\nu 2s_{1/2}$	0.03	0.09	—	0.02	0.12	—
$\pi 0f_{7/2}$	7.46	7.19	—	7.41	6.94	—
$\pi 1p$	2.11	2.17	1.77 ± 0.15	3.29	2.69	2.08 ± 0.15
$\pi 0f_{5/2}$	2.16	2.30	2.04 ± 0.25	2.98	2.63	3.16 ± 0.25
$\pi 0g_{9/2}$	0.17	0.19	0.23 ± 0.25	0.21	1.16	0.84 ± 0.25
$\pi 1d_{5/2}$	0.03	0.05	—	0.04	0.25	—
$\pi 0g_{7/2}$	0.06	0.09	—	0.08	0.15	—
$\pi 1d_{3/2}$	0.02	0.03	—	0.02	0.05	—
$\pi 2s_{1/2}$	0.01	0.01	—	0.01	0.03	—

model-dependencies both in the theoretical and experimental values [55]. Such a comparison is therefore useful in qualitative terms.

4. Summary and outlook

In this work a detailed study of the low-lying structure of the nuclei ^{76}Ge and ^{76}Se calculated with SCCM methods has been presented. These two isobars are of a great deal of interest because they are the initial and final nuclei in one of the most promising neutrinoless double-beta decay experiments. The present SCCM methods include particle number and angular momentum projections, as well as quadrupole shape mixing within the GCM framework. Energy levels, electromagnetic properties, c.w.f.s and occupation numbers of spherical single-particle orbits have been analyzed.

The main conclusion of the present study is that both nuclei are triaxial deformed and the axial approximation only captures part of such a triaxial structure by mixing prolate and oblate configurations that are indeed saddle points in the (β_2, γ) plane. The comparison with the experimental data is rather good when triaxial deformations are included in the calculation. Hence, the triaxial calculations are able to reproduce qualitatively the appearance of γ-bands in ^{76}Ge and ^{76}Se, the more γ-rigid character of ^{76}Ge and the more transitional character of ^{76}Se and the correct spectroscopic quadrupole moments of the 2_1^+ states in both nuclei. However, the transition probabilities are systematically larger than the experimental ones, probably because of the overestimation of the deformation with the Gogny D1S interaction when the angular momentum projection is taken into account. A more quantitative agreement both in the energies and in the transition probabilities is expected if other degrees of freedom

are included in the present SCCM framework, especially cranking terms [64, 69]. Some work is in progress in this direction.

The role of the *pf* and *gds* spherical single-particle orbits has been also analyzed by computing the occupation numbers with the ground state wave functions. This study has shown that the filling in of the quadrupole partner and the spin–orbit partner of the $g_{9/2}$ orbit, i.e., the $d_{5/2}$ and $g_{7/2}$ orbits, and the removal of protons in the $f_{7/2}$ orbit, are small but not completely negligible. Therefore, LSSM calculations including some–or all–of these orbits in the active valence space would be of interest for the computation of $0\nu\beta\beta$ NMEs.

As a concluding remark, the present work shows the relevance of the triaxial degree of freedom in these two nuclei that are involved in $0\nu\beta\beta$ decays. Since only axial calculations have been used so far to compute NMEs within the EDF framework, it is important to include triaxial deformations in the near future to study their impact on this important quantity and also in the description of charge-exchange reactions [70, 71]. Work is in progress along these lines.

Acknowledgments

I gratefully thank the support from GSI-Darmstadt computing facility. This work was supported by the Spanish Ministerio de Economía y Competitividad under contracts Programa Ramón y Cajal 2012 No. 11420 and FIS-2014-53434-P.

References

[1] Suhonen J and Civitarese O 1998 *Phys. Rep.* **300** 123
[2] Avignone F T, Elliott S R and Engel J 2008 *Rev. Mod. Phys.* **80** 481
[3] Vergados J D, Ejiri H and Simkovic F 2012 *Rep. Prog. Phys.* **75** 106301
[4] Caurier E, Menéndez J, Nowacki F and Poves A 2008 *Phys. Rev. Lett.* **100** 052503
[5] Menéndez J, Caurier E, Nowacki F and Poves A 2009 *Nucl. Phys.* A **100** 139
[6] Horoi M and Stoica S 2010 *Phys. Rev.* C **81** 024321
[7] Sen'kov R A and Horoi M 2016 *Phys. Rev.* C **93** 044334
[8] Iwata Y, Shimizu N, Otsuka T, Utsuno Y, Menéndez J, Honma M and Abe T 2016 *Phys. Rev. Lett.* **116** 112502
[9] Simkovic F, Pantis G, Vergados J D and Faessler A 1999 *Phys. Rev.* C **60** 055502
[10] Simkovic F, Faessler A, Rodin V, Vogel P and Engel J 2008 *Phys. Rev.* C **77** 045503
[11] Kortelainen M and Suhonen J 2007 *Phys. Rev.* C **75** 051303
[12] Suhonen J and Civitarese O 2010 *Nucl. Phys.* A **847** 207
[13] Barea J and Iachello F 2009 *Phys. Rev.* C **79** 044301
[14] Barea J, Kotila J and Iachello F 2013 *Phys. Rev.* C **87** 014315
[15] Rodríguez T R and Martínez-Pinedo G 2010 *Phys. Rev. Lett.* **105** 252503
[16] López-Vaquero N, Rodríguez T R and Egido L 2013 *Phys. Rev. Lett.* **111** 142501
[17] Song L S, Yao J M, Ring P and Meng J 2014 *Phys. Rev.* C **90** 054309
[18] Yao J M, Song L S, Hagino K, Ring P and Meng J 2015 *Phys. Rev.* C **91** 024316
[19] Vogel P 2012 *J. Phys. G: Nucl. Part. Phys.* **39** 124002
[20] Engel J 2015 *J. Phys. G: Nucl. Part. Phys.* **42** 034017
[21] Menéndez J, Poves A, Caurier E and Nowacki F 2008 (arXiv:0809.2183)
[22] Fang D-L, Faessler A, Rodin V and Simkovic F 2011 *Phys. Rev.* C **83** 034320
[23] Mustonen M T and Engel J 2013 *Phys. Rev.* C **87** 064302
[24] Yao J M and Engel J 2016 *Phys. Rev.* C **94** 014306
[25] Hinohara N and Engel J 2014 *Phys. Rev.* C **90** 031301
[26] Simkovic F, Rodin V, Faessler A and Vogel P 2013 *Phys. Rev.* C **87** 045501
[27] Menéndez J, Rodríguez T R, Martínez-Pinedo G and Poves A 2014 *Phys. Rev.* C **90** 024311
[28] Barea J, Kotila J and Iachello F 2015 *Phys. Rev.* C **91** 034304
[29] Horoi M and Brown B A 2013 *Phys. Rev. Lett.* **110** 222502

[30] Simkovic F, Hodak R, Faessler A and Vogel P 2011 *Phys. Rev.* C **83** 015502
[31] Sen'kov R A and Horoi M 2013 *Phys. Rev.* C **88** 064312
[32] Rodríguez T R and Martinez-Pinedo G 2013 *Phys. Lett.* B **719** 174
[33] Menéndez J, Hinohara N, Engel J, Martínez-Pinedo G and Rodríguez T R 2016 *Phys. Rev.* C **93** 014305
[34] Agostini M *et al* (GERDA Collaboration) 2013 *Phys. Rev. Lett.* **111** 122503
[35] Abgrall N *et al* 2014 *Adv. High Energy Phys.* **2014** 1
[36] Bender M and Heenen P-H 2008 *Phys. Rev.* C **78** 024309
[37] Rodríguez T R and Egido J L 2010 *Phys. Rev.* C **81** 064323
[38] Yao J M, Meng J, Ring P and Vretenar D 2010 *Phys. Rev.* C **81** 044311
[39] Berger J F, Girod M and Gogny D 1984 *Nucl. Phys.* A **428** 23
[40] Rodríguez T R, Poves A and Nowacki F 2016 *Phys. Rev.* C **93** 054316
[41] Toh Y *et al* 2013 *Phys. Rev.* C **87** 041304(R)
[42] Davydov A S and Filippov G F 1958 *Nucl. Phys.* **8** 237
[43] Bhat G H, Dar W A, Sheikh J A and Sun Y 2014 *Phys. Rev.* C **89** 014328
[44] Zhang D-L and Ding B-G 2013 *Chin. Phys. Lett.* **30** 122101
[45] Nikšić T, Marević P and Vretenar D 2014 *Phys. Rev.* C **89** 044325
[46] Lecomte R *et al* 1977 *Nucl. Phys.* A **284** 123
[47] Ballester F, Casal E, England J B A and Moriano F 1988 *J. Phys. G: Nucl. Phys.* **14** 11031
[48] Xu C *et al* 2015 *Phys. Rev.* C **91** 061303
[49] Barfield A F and Lieb K P 1990 *Phys. Rev.* C **41** 1762
[50] Deloncle I, Libert J, Bennour L and Quentin P 1989 *Phys. Lett.* B **233** 16
[51] Hilaire S and Girod M 2006 http://www-phynu.cea.fr/science_en_ligne/carte_potentiels_microscopiques/carte_potentiel_nucleaire_eng.htm
[52] Rodríguez T R and Martínez-Pinedo G 2011 *Prog. Part. Nucl. Phys.* **66** 436
[53] Schiffer J P *et al* 2008 *Phys. Rev. Lett.* **100** 112501
[54] Kay B P *et al* 2009 *Phys. Rev.* C **79** 021301(R)
[55] Duguet T, Hergert H, Holt J D and Somà V 2015 *Phys. Rev.* C **92** 034313
[56] Menéndez J, Poves A, Caurier E and Nowacki F 2009 *Phys. Rev.* C **80** 048501
[57] Suhonen J and Civitarese O 2008 *Phys. Lett.* B **668** 277
[58] Simkovic F, Faessler A and Vogel P 2009 *Phys. Rev.* C **79** 015502
[59] Ring P and Schuck P 1980 *The Nuclear Many Body Problem* (Berlin: Springer)
[60] Anguiano M, Egido J L and Robledo L M 2001 *Nucl. Phys.* A **696** 467
[61] Bender M, Heenen P-H and Reinhard P-G 2003 *Rev. Mod. Phys.* **75** 121
[62] Rodríguez-Guzmán R, Egido J L and Robledo L M 2002 *Nucl. Phys.* A **709** 201
[63] Rodríguez T R 2016 *Eur. Phys. J.* A **52** 190
[64] Borrajo M, Rodríguez T R and Egido J L 2015 *Phys. Lett.* B **746** 341
[65] Wilets L and Jean M 1956 *Phys. Rev.* **102** 788
[66] Zamfir N V and Casten R F 1991 *Phys. Lett.* B **260** 265
[67] ENSDF Database www.nndc.bnl.gov/ensdf/
[68] Lie S G and Holzwarth J 1975 *Phys. Rev.* C **12** 1035
[69] Borrajo M and Egido J L 2015 *Acta Phys. Pol.* B **8** 567
[70] Grewe E-W *et al* 2008 *Phys. Rev.* C **78** 044301
[71] Thies J H *et al* 2012 *Phys. Rev.* C **86** 014304